SAND2006-5488P

Peridynamics via Finite Element Analysis

By

Richard W. Macek, Los Alamos National Laboratory
Stewart A. Silling, Sandia National Laboratories

Abstract

The peridynamic theory of solid mechanics replaces the partial differential equations of the classical theory with integral equations. These integral equations remain valid in the presence of discontinuities such as cracks and therefore offer the potential to model fracture with great generality. In previous work, a discretized form of the peridynamic integral equations was implemented in a meshless code called EMU. The present paper describes how the peridynamic model can also be implemented in a conventional finite element code using truss elements. This implementation allows different subregions of a model to solve either the classical partial differential equations or the peridynamic equations in the same calculation. Several example problems involving fracture and damage demonstrate the utility and robustness of peridynamics. It is also shown that the peridynamic model, as implemented in the ABAQUS finite element code, gives essentially the same results as EMU. The availability of the peridynamic model in a finite element (FE) code allows a penetrator to be modeled with a conventional FE mesh, while the target is modeled as peridynamic.

Introduction

Numerical prediction of crack growth and damage are long-standing problems in computational mechanics. The difficulties inherent in these problems arise from the basic incompatibility of cracks with the partial differential equations that are used in the classical theory of solid mechanics. The spatial derivatives needed for these partial differential equations to make sense do not exist on a crack tip or surface. Therefore, any numerical method derived from these equations inherits this difficulty in modeling cracks. Typically such methods also require supplemental relations that govern the initiation, as well as the growth velocity and direction, of cracks. These relations must be applied along each crack tip, leading to the inherent complexity of the method, particularly when multiple cracks occur and interact in three dimensions. As an attempt at improving this situation, a theory of solid mechanics has been proposed that does not require spatial derivatives to be evaluated within a body.[1–6] This theory, known as the *peridynamic* theory, instead uses integral equations. The objective is to reformulate the basic mathematical description of solid mechanics in such a way that the identical equations hold either on or off of a discontinuity such as a crack. This paper is a discussion of the peridynamic continuum theory as well as the basic numerical equations used in the EMU code[7] that implements this continuum model. In addition, it is shown that the basic peridynamic equations are entirely consistent with even the most fundamental finite element analysis (FEA) code architectures. In fact, within the FEA framework, coupling peridynamics to conventional FEA models is very possible. This paper presents several examples that demonstrate this equivalency and show the ease of

implementing peridynamics in a finite element (FE) code. Given the popularity and utility of FEA, this latter realization may significantly expand the applicability of peridynamics.

Peridynamic Model of a Continuum

The peridynamic theory may be thought of as a continuum version of molecular dynamics. The acceleration of any particle at $\mathbf{x}$ in the reference configuration at time t is found from

$$\rho\ddot{\mathbf{u}}(\mathbf{x},t) = \int_{H_{\mathbf{x}}} \mathbf{f}(\mathbf{u}(\mathbf{x}',t)-\mathbf{u}(\mathbf{x},t),\mathbf{x}'-\mathbf{x})dV_{\mathbf{x}'} + \mathbf{b}(\mathbf{x},t), \qquad (1)$$

where $H_{\mathbf{x}}$ is a neighborhood of $\mathbf{x}$, $\mathbf{u}$ is the displacement vector field, $\mathbf{b}$ is a prescribed body force density field, ρ is mass density in the reference configuration, and $\mathbf{f}$ is a *pairwise force function* whose value is the force vector (per unit volume squared) that the particle $\mathbf{x}'$ exerts on the particle $\mathbf{x}$. In the following discussion, we denote the relative position of these two particles in the reference configuration by $\boldsymbol{\xi}$:

$$\boldsymbol{\xi} = \mathbf{x}'-\mathbf{x} \qquad (2)$$

and their relative displacement by $\boldsymbol{\eta}$:

$$\boldsymbol{\eta} = \mathbf{u}(\mathbf{x}',t)-\mathbf{u}(\mathbf{x},t). \qquad (3)$$

Note that $\boldsymbol{\eta}+\boldsymbol{\xi}$ represents the current relative position vector connecting the particles.

The direct physical interaction (which occurs through unspecified means) between the particles at $\mathbf{x}$ and $\mathbf{x}'$ will be called a *bond*, or in the special case of an elastic interaction to be defined, a *spring*. The concept of a bond that extends over a finite distance is a fundamental difference between the peridynamic theory and the classical

theory, which is based on the idea of contact forces (interactions between particles that are in direct contact with each other).

Constitutive Modeling

It is convenient to assume that for a given material there is a positive number δ, called the *horizon*, such that

$$|\boldsymbol{\xi}| > \delta \Rightarrow \mathbf{f}(\boldsymbol{\eta}, \boldsymbol{\xi}) = 0 \qquad \forall \boldsymbol{\eta}. \tag{4}$$

In other words, the particle **x** cannot "see" beyond this horizon. For the remainder of this discussion, $H_{\mathbf{x}}$ will denote the spherical neighborhood of **x** in R with radius δ (Figure 1).

The pairwise force function **f** is required to have the following properties:

$$\mathbf{f}(-\boldsymbol{\eta}, -\boldsymbol{\xi}) = -\mathbf{f}(\boldsymbol{\eta}, \boldsymbol{\xi}) \quad \forall \boldsymbol{\eta}, \boldsymbol{\xi}, \tag{5}$$

which ensures conservation of linear momentum, and

$$(\boldsymbol{\xi} + \boldsymbol{\eta}) \times \mathbf{f}(\boldsymbol{\eta}, \boldsymbol{\xi}) = \mathbf{0} \quad \forall \boldsymbol{\eta}, \boldsymbol{\xi}, \tag{6}$$

which ensures conservation of angular momentum. The latter equation means that the force vector between any two particles is parallel to the particles' current relative position vector.

A material is said to be *microelastic* if the pairwise force function is derivable from a scalar *micropotential* w:

$$\mathbf{f}(\boldsymbol{\eta}, \boldsymbol{\xi}) = \frac{\partial w}{\partial \boldsymbol{\eta}}(\boldsymbol{\eta}, \boldsymbol{\xi}) \quad \forall \boldsymbol{\xi}, \boldsymbol{\eta}. \tag{7}$$

The micropotential is the energy in a single bond and has dimensions of energy per unit volume squared. The energy per unit volume in the body at a given point (i.e., the local strain energy density) is therefore found from

$$W = \frac{1}{2}\int_{H_{\mathbf{x}}} w(\boldsymbol{\eta},\boldsymbol{\xi})\,dV_{\boldsymbol{\xi}}. \tag{8}$$

The factor of 1/2 appears because each endpoint of a bond "owns" only half the energy in the bond.

If a body is composed of a microelastic material, work done on it by external forces is stored in recoverable form in much the same way as in the classical theory of elasticity. Furthermore, it can be shown that the micropotential depends on the relative displacement vector $\boldsymbol{\eta}$ only through the scalar distance between the deformed points. Thus, there is a scalar-valued function $\hat{w}$ such that

$$\hat{w}(y,\boldsymbol{\xi}) = w(\boldsymbol{\eta},\boldsymbol{\xi}) \quad \forall \boldsymbol{\xi},\boldsymbol{\eta}, \quad y = |\boldsymbol{\eta}+\boldsymbol{\xi}|. \tag{9}$$

Therefore, the interaction between any two points in a microelastic material may be thought of as an elastic (and possibly nonlinear) spring. The spring properties may depend on the separation vector $\boldsymbol{\xi}$ in the reference configuration.

Anisotropy may be included in the microelastic response through this dependence on the direction of $\boldsymbol{\xi}$. For example, in formulating a model of a unidirectional fiber-reinforced composite material in which the fibers are parallel to a given unit vector **g**, one might take

$$\hat{w}(y,\boldsymbol{\xi}) = \beta^2 \hat{w}_{\text{fiber}}(y,|\boldsymbol{\xi}|) + (1-\beta^2)\hat{w}_{\text{matrix}}(y,|\boldsymbol{\xi}|), \quad \beta = \frac{\mathbf{g}\cdot\boldsymbol{\xi}}{|\boldsymbol{\xi}|}, \tag{10}$$

which explicitly supplies the dependence of bond energy on the bond direction. Combining Eqs. (7) and (9) and differentiating the latter with respect to the components of $\boldsymbol{\eta}$ leads to

$$\mathbf{f}(\boldsymbol{\eta},\boldsymbol{\xi}) = \frac{\boldsymbol{\xi}+\boldsymbol{\eta}}{|\boldsymbol{\xi}+\boldsymbol{\eta}|} f(|\boldsymbol{\xi}+\boldsymbol{\eta}|,\boldsymbol{\xi}) \quad \forall \boldsymbol{\xi},\boldsymbol{\eta}, \tag{11}$$

where f is the scalar-valued function defined by

$$f(y,\boldsymbol{\xi}) = \frac{\partial \hat{w}}{\partial y}(y,\boldsymbol{\xi}) \quad \forall y,\boldsymbol{\eta}. \tag{12}$$

This satisfies the requirements of Eqs. (5) and (6), provided

$$\hat{w}(y,-\boldsymbol{\xi}) = \hat{w}(y,\boldsymbol{\xi}) \quad \forall y,\boldsymbol{\xi}, \tag{13}$$

which will henceforth be assumed.

The relation shown in Eq. (11), together with the equation of motion, Eq. (1), essentially contains the totality of the peridynamic model for a nonlinear microelastic material. In particular, note that the issue of how to treat rigid rotation does not arise in this formulation because y is invariant under rotation of the body. Similarly, objectivity of a constitutive model is not an issue in this approach.

Proportional Microelastic Materials

In the *proportional* microelastic material, the bond force f varies linearly with *bond stretch* s, defined by

$$s = \frac{|\boldsymbol{\xi}+\boldsymbol{\eta}| - |\boldsymbol{\xi}|}{|\boldsymbol{\xi}|} = \frac{y - |\boldsymbol{\xi}|}{|\boldsymbol{\xi}|}. \tag{14}$$

Thus s is positive when the bond is in tension. The bond force in the proportional microelastic material is given by

$$f(y(t),\boldsymbol{\xi}) = g(s(t,\boldsymbol{\xi}),|\boldsymbol{\xi}|), \tag{15}$$

where g is the scalar-valued function given by

$$g(s,|\boldsymbol{\xi}|) = \begin{cases} cs & \text{if } |\boldsymbol{\xi}| \le \delta \\ 0 & \text{otherwise} \end{cases}, \tag{16}$$

where c is a constant called the *spring constant*. Alternative forms of g are possible in the peridynamic theory but have not yet been studied in detail.

To determine c from a given bulk modulus k, consider a large homogeneous body under isotropic extension, i.e., s is constant for all $\boldsymbol{\xi}$, and $\boldsymbol{\eta} = s\boldsymbol{\xi}$. Defining $\xi = |\boldsymbol{\xi}|$ and $\eta = |\boldsymbol{\eta}|$, we have $\eta = s\xi$. Using the definition of the micropotential shown in Eq. (7), since $f = cs = c\eta/\xi$, it follows that $w = c\eta^2/2\xi = cs^2\xi/2$. Then, applying Eq. (8) leads to

$$W = \frac{1}{2}\int_H w dV_{\boldsymbol{\xi}} = \frac{1}{2}\int_0^\delta \left(\frac{cs^2\xi}{2}\right) 4\pi\xi^2 d\xi = \frac{\pi c s^2 \delta^4}{4}. \tag{17}$$

This is required to equal the strain energy density in the classical theory of elasticity for the same material and the same deformation, $W = 9ks^2/2$. Combining this requirement with Eq. (17) leads to the spring constant in the proportional microelastic material model,

$$c = \frac{18k}{\pi\delta^4}. \tag{18}$$

Proportional Microplastic Materials

This material model is similar to the proportional microelastic model, but it includes plasticity (permanent deformation) at the bond level. The history dependence is included by modifying Eq. (15) as follows:

$$f(y(t), |\boldsymbol{\xi}|, t) = g(s(t, \boldsymbol{\xi}), |\boldsymbol{\xi}|, t), \tag{19}$$

where g is the scalar-valued function given by

$$g(s, |\boldsymbol{\xi}|, t) = \begin{cases} c(s - \bar{s}(t)) & \text{if } |\boldsymbol{\xi}| \le \delta \\ 0 & \text{otherwise,} \end{cases} \tag{20}$$

and where

$$\bar{s}(0) = 0, \quad \dot{\bar{s}} = \begin{cases} \dot{s} & \text{if} |s - \bar{s}| \le s_Y \\ 0 & \text{otherwise.} \end{cases} \tag{21}$$

Here s_Y is a constant that represents the stretch at which a bond yields (in either tension or compression). Thus s_Y is called the *yield stretch* for bonds. Note that according to

Eqs. (19), (20), and (21), $-cs_Y \le f \le cs_Y$ for all time. Figure 2 illustrates a possible loading path and resulting permanent deformation in the bond.

Damage

The simplest way to introduce failure into a constitutive model is by allowing bonds (springs) to break when they are stretched beyond a predefined limit. After bond failure, there is no tensile force sustainable in the bond. Once a bond fails, it is failed forever (there is no provision for "healing" of a failed bond); this makes the model history dependent. For purposes of illustration, consider the *prototype microelastic brittle* (PMB) material. This is a modification of the proportional microelastic material to include damage. It is defined by

$$f(y(t),\boldsymbol{\xi},t) = g(s(t,\boldsymbol{\xi}),|\boldsymbol{\xi}|)\mu(t,\boldsymbol{\xi}), \tag{22}$$

where g is the linear scalar-valued function given by

$$g(s,|\boldsymbol{\xi}|) = \begin{cases} cs & \text{if } |\boldsymbol{\xi}| \le \delta \\ 0 & \text{otherwise,} \end{cases} \tag{23}$$

where c is a constant, and μ is a history-dependent scalar-valued function that takes on values of either 1 or 0:

$$\mu(t,\boldsymbol{\xi}) = \begin{cases} 1 & \text{if } s(t',\boldsymbol{\xi}) < s_0 \text{ for all } 0 \le t' \le t \\ 0 & \text{otherwise.} \end{cases} \tag{24}$$

Here, s_0 is the critical stretch for bond failure, which for the moment will be assumed constant (Figure 3). Note that although the PMB material is isotropic in its virgin state, breakage of bonds oriented in some particular direction will lead to anisotropy in subsequent response. One advantage of introducing failure at the bond level is that it leads to an unambiguous notion of local damage at a point, which is defined as

$$\varphi(\mathbf{x},t) = \frac{1 - \int_{H_\mathbf{x}} \mu(\mathbf{x},t,\boldsymbol{\xi}) dV_\boldsymbol{\xi}}{\int_{H_\mathbf{x}} dV_\boldsymbol{\xi}}, \tag{25}$$

in which **x** is now included as an argument of μ as a reminder that it is a function of position in the body. Note that $0 \le \varphi \le 1$, with 0 representing virgin material and 1 representing complete disconnection of a point from all of the points with which it initially interacted.

Because broken bonds are unable to sustain tensile load, the onset of bond breakage at some point in a body leads to a softening material response. This may cause an evolution of damage in which broken bonds coalesce into a surface that becomes a fracture, with extensive bond breakage across the surface. (The precise mathematical condition for material instability with regard to damage evolution is an open question at this time. Such a criterion appears to be more complex in the present setting than is loss of ellipticity in partial differential equations, especially because of the directional nature of damage due to bond failure introduced through $\mu(\mathbf{x},t,\boldsymbol{\xi})$.)

The critical stretch for bond failure, s_0, may be obtained from a measurable quantity by considering a planar fracture surface in the interior of a large homogeneous body. To completely separate the two halves of the body across the fracture surface requires breaking all the bonds that initially connected points in the opposite halves. Let $w_0(\xi)$ denote the work (per unit volume squared) required to break a single bond of length ξ.

$$w_0(\xi) = \int_0^{s_0} g(s)(\xi ds), \qquad \xi = |\boldsymbol{\xi}|, \tag{26}$$

where the relation $d\eta = \xi ds$ has been used. In the present case of the PMB material,

Eq. (26) leads to $w_0(\xi) = cs_0^2\xi/2$. The work G_0 required to break all the bonds per unit fracture area is then found from

$$G_0 = \int_0^{\delta}\int_0^{2\pi}\int_z^{\delta}\int_0^{\cos^{-1} z/\xi}(cs_0^2\xi/2)\xi^2\sin\phi\, d\phi\, d\xi\, d\theta\, dz. \tag{27}$$

(Refer to Figure 4 for an explanation of this computation.) After evaluation of these integrals for the PMB material, the energy per unit fracture area for complete separation of the two halves of the body is found to be

$$G_0 = \frac{\pi c s_0^2 \delta^5}{10}. \tag{28}$$

Since the energy release rate is a measurable quantity for brittle materials, Eq. (28) allows s_0 to be evaluated under the assumptions of complete separation of the fracture surfaces and of the absence of other dissipative mechanisms near the crack tip. Solving Eq. (28) for s_0 and using Eq. (18) lead to

$$s_0 = \sqrt{\frac{10G_0}{\pi c\delta^5}} = \sqrt{\frac{5G_0}{9k\delta}}. \tag{29}$$

This determines s_0 for the PMB material under the assumptions stated above. For microplastic materials that can undergo damage, the expression for w_0 in Eq. (26) must be modified, and the resulting integration in Eq. (27) can be performed numerically.

Bond Properties for Interfaces

Interfaces between materials are characterized through the properties of bonds that connect points in the different materials. The properties of these interface bonds can be chosen independently of the bonds within the individual materials. For example, a weak interface would be modeled by reducing s_0 for the bonds across the interface.

The spring constant of interface bonds $c^{m,n}$ connecting materials m and n represents those of an adhesive, if such an adhesive is present. The same relation for a

homogeneous material, Eq. (18), may be used for this. Otherwise, it is reasonable to set

$$c^{m,n} = \frac{c^m + c^n}{2}, \tag{30}$$

where c_m and c_n are the spring constants of the individual materials. Similarly, the value of critical bond stretch for breakage of interface bonds may be found from the same expression, Eq. (29)**,** as for homogeneous materials. However, a more appropriate value may be

$$s_0^{m,n} = \min(s_0^m, s_0^n), \tag{31}$$

which is based on the assumption that the weaker material determines the strength of the bonds across an interface.

Comparison with Classical Material Models

The model described above allows only one elastic constant, called *c*, in the case of the PMB material, whereas isotropic linear elastic materials in the classical theory are characterized by two such constants. This difference occurs because an elastic solid that involves only two-particle interactions (a "Cauchy crystal") always has a Poisson ratio of 1/4. A refinement of the peridynamic theory that allows dependence of strain energy density on local volume change in addition to two-particle interactions removes this restriction[1] and can be implemented to model fluids. Indeed, allowing the bond properties to depend not only on the stretch in that bond itself but also on the stretch of all bonds connected to its end points may permit more general constitutive models in the peridynamic theory.

Another aspect of constitutive modeling in the peridynamic theory that has no analogue in the classical theory is the dependence of f on $\boldsymbol{\xi}$. For the virgin PMB material, it was assumed for convenience that f depends only on *s*, which implies a

particular dependence on $\boldsymbol{\xi}$. However, many alternatives are possible, and it is shown in Ref. 1 that the nature of this dependence affects the dispersion relation of the material for linear waves. This can potentially be exploited in the nanoscale modeling of materials.

Short-Range Forces

In the theory discussed so far, particles interact only through peridynamic bonds. Therefore, particles that are separated in the reference configuration by distances greater than the horizon δ do not interact because of Eq. (4). However, in practice, many applications involve multiple bodies that initially are separated by a large (compared with δ) distance but eventually come into contact. The theory developed so far cannot encompass contact forces.

To allow for contact forces, *short-range* forces are now introduced. These forces do not depend on the distance between particles in the reference configuration, only on their relative position in the current configuration. Specifically, it is assumed that

$$\mathbf{f}_s(\mathbf{y}',\mathbf{y}) = \frac{\mathbf{y}'-\mathbf{y}}{|\mathbf{y}'-\mathbf{y}|}\min\left\{0, c_s\left(\frac{|\mathbf{y}'-\mathbf{y}|}{2r_s}-1\right)\right\}, \tag{32}$$

where c_s and r_s are positive constants, and $\mathbf{y}$ and $\mathbf{y}'$ are the deformed positions of $\mathbf{x}$ and $\mathbf{x}'$ respectively,

$$\mathbf{y} = \mathbf{x} + \mathbf{u}, \quad \mathbf{y}' = \mathbf{x}' + \mathbf{u}'. \tag{33}$$

Thus, short-range forces are nonzero only when the two particles are closer to each other than $2r_s$. For this reason, r_s is called the node radius. Short-range forces can be only compressive (repulsive), according to Eq. (32).

For proportional materials, the value of c_s can be chosen to be some multiple of c, where c is the spring constant of the material. The multiple depends on the desired

stiffness of the contact forces. A suitable default, which results in a stiffness close to that of the bulk elastic properties of the material, is

$$c_s = 15c. \tag{34}$$

Force Normalization at Surfaces

It was shown in Eq. (18) that the spring constant can be obtained from the bulk elastic modulus for a real material. However, the derivation that leads to this result assumed that a given material particle has surrounding it a spherical neighborhood of radius δ completely filled with the same material. This assumption does not hold if the particle is within a distance δ of a free surface or an interface with some other material. If the spring constant given by Eq. (18) is used for such points, the resulting body would have incorrect bulk elastic properties.

To account for this effect near free surfaces and interfaces, a correction called force normalization is used. In this method, if **X** is a point in the body, possibly near a surface, let the tensor **P(X)** be defined by

$$\mathbf{P(X)} = \frac{\partial}{\partial \mathbf{U}} \int_{H_{\mathbf{X}}} \mathbf{f(U, X - x')} dV_{\mathbf{x}'} . \tag{35}$$

Thus $-\mathbf{P(X)}\Delta\mathbf{u}$ equals the restoring force (per unit volume) that the particle **X** experiences if it is displaced incrementally through a small vector $\Delta\mathbf{u}$ while holding all other points fixed. It can be shown that **P** is a symmetric tensor[1] that is also positive definite for reasonably behaved materials. Therefore, **P** has three positive eigenvalues $\{p^1, p^2, p^3\}$. Let p^1 be the largest of these. Further, let $\mathbf{P}_\infty$ be the analogous tensor obtained for a large homogeneous body (in contrast to **P(X)**, which takes into account the particular location of **X**). The eigenvalues of $\mathbf{P}_\infty$ are denoted $\left\{p_\infty^1, p_\infty^2, p_\infty^3\right\}$, with p_∞^1 being the largest of the

three.

Let c_∞ be the spring constant obtained from Eq. (18), i.e., the value appropriate for a large homogeneous body composed of the material that is present at **X**. Then the modified spring constant $c(\mathbf{X})$, taking into account surfaces and interfaces near point **X**, is set to

$$c(\mathbf{X}) = \frac{c_\infty p^1_\infty}{p^1(\mathbf{X})}. \tag{36}$$

In general, $c(\mathbf{X}) \geq c_\infty$. The assumption in this force normalization method is that the local stiffness scales according to the eigenvalues of the **P** tensor. This method has been found to provide the correct bulk elastic response in thin structures (in which free surfaces are important) and in bodies containing planar surfaces.

Direct Numerical Method

This section presents a summary of the numerical approximation to the peridynamic equations that is used in the EMU code.[4] The region is discretized into nodes, each with a known volume in the reference configuration. Taken together, the nodes form a grid. In EMU the method is mesh free in the sense that there are no elements or other geometrical connections between the nodes. However, in FEA the peridynamic grid becomes an assemblage of nonlinear trusses. For simplicity, the details of the method implemented in EMU are discussed here using the linearized version of the peridynamic theory applied to a homogeneous body. The discretized form of the equation of motion (1) replaces the integral by a finite sum:

$$\rho \ddot{\mathbf{u}}_i^n = \sum_p \mathbf{f}(\mathbf{u}_p^n - \mathbf{u}_i^n, \mathbf{x}_p - \mathbf{x}_i) V_p + \mathbf{b}_i^n, \tag{37}$$

where **f** is supplied by Eq. (11), n is the time step number, and subscripts denote the node

number, so that

$$\mathbf{u}_i^n = \mathbf{u}(\mathbf{x}_i, t^n). \tag{38}$$

In Eq. (37) V_p is the volume of node p, which for a uniform rectangular gird is simply Δx^3. The sum in Eq. (37) is taken over all nodes p such that $|x_p - x_i| < \delta$. The discretized equation of motion, Eq. (37), is easy to implement in its fully nonlinear form. However, for purposes of error analysis and numerical stability analysis, it is necessary to work with a linearized version. The discretized form of the linearized peridynamic model is

$$\rho\ddot{\mathbf{u}}_i^n = \sum_p \mathbf{C}(\mathbf{x}_p - \mathbf{x}_i)(\mathbf{u}_p^n - \mathbf{u}_i^n)V_p + \mathbf{b}_i^n, \tag{39}$$

where $\mathbf{C}$ is a tensor-valued function called the *micromodulus* defined by

$$\mathbf{C}(\boldsymbol{\xi}) = \frac{\partial \mathbf{f}}{\partial \boldsymbol{\eta}}(\mathbf{0}, \boldsymbol{\xi}) \quad \forall \boldsymbol{\xi}. \tag{40}$$

Hence, the pairwise force in the linearized theory is given by $\mathbf{f} = \mathbf{C}(\boldsymbol{\xi})\boldsymbol{\eta}$. For the special case of proportional materials, it follows from Eqs. (14), (15), (16), and (40) that

$$\mathbf{C}(\boldsymbol{\xi}) = c\frac{\boldsymbol{\xi} \otimes \boldsymbol{\xi}}{|\boldsymbol{\xi}|^3} \qquad \text{or} \qquad C_{ij}(\boldsymbol{\xi}) = c\frac{\xi_i \xi_j}{(\xi_k \xi_k)^{3/2}}, \tag{41}$$

where the latter expression uses components in a Cartesian coordinate frame. An explicit central difference formula is used for acceleration in either Eq. (37) or Eq. (39):

$$\rho\ddot{\mathbf{u}}_i^n = \frac{\mathbf{u}_i^{n+1} - 2\mathbf{u}_i^n + \mathbf{u}_i^{n-1}}{\Delta t^2}. \tag{42}$$

Through the use of standard error analysis techniques,[4] the spatial and temporal discretization errors associated with Eq. (39) can be shown to be $O(\Delta x^2) + O(\Delta t^2)$. In addition, von Neumann stability analysis[8] of Eq. (39) leads to a stable time step

requirement of

$$\Delta t < \sqrt{\frac{2\rho}{\sum_p V_p \left|\mathbf{C}(\mathbf{x}_p - \mathbf{x}_i)\right|}}. \tag{43}$$

The value of the horizon δ may depend on the physical nature of the application being modeled. For example, at the nanoscale, δ would be determined by the distance over which physical interaction between atoms or molecules occurs. However, in macroscale calculations, δ can be chosen according to convenience, since, as shown previously, the parameters such as c that determine the bulk elastic properties of the material can be fitted to experimental data for any value of δ. See, for example, Eq. (18). In practice, for macroscale modeling, the value $\delta = 3\Delta x$ usually works well. Values much smaller than this typically result in undesirable grid effects (cracks grow along the rows or columns of the grid). Values much larger than this may result in excessive wave dispersion and require very large computer run times.

Boundary conditions are somewhat different in the peridynamic method than in the classical theory. As shown in Ref. 1, the variational formulation of the peridynamic equations does not lead to natural boundary conditions, which in the classical theory are traction boundary conditions. Instead, forces at the surface of a body must be applied as body forces **b** within some layer under the surface. In practice, this layer usually has thickness δ. Similarly, displacement boundary conditions must be prescribed within a layer of finite thickness under the surface.

Although the above analysis assumes a regular lattice of nodes, the method is not restricted to such structured grids. Through the use of irregular grids, complex geometries may be modeled, and the full advantages of a meshless method are realized.

Finite Element Implementation

Recall that the interaction between the particles of a peridynamic continuum occurs through bonds that represent the physical force between pairs of particles. The totality of all such bonds forms a network within a body that connects all pairs of particles that interact with each other. Such a network of the bonds is Lagrangian in the sense that the bonds are defined in the reference (undeformed) configuration; therefore, the connectivity does not change during deformation.

Although the discretization in EMU described in the previous section is meshless, for purposes of implementation in a finite element code, a mesh made of truss elements with the appropriate stiffness properties is used to represent the peridynamic bonds. To do this, first observe that multiplying Eq. (37) by V_i leads to the standard equation of motion for finite element analysis (FEA):

$$V_i \rho \ddot{\mathbf{u}}_i^n = \sum_p \mathbf{f}(\mathbf{u}_p^n - \mathbf{u}_i^n, \mathbf{x}_p - \mathbf{x}_i) V_p V_i + \mathbf{b}_i^n V_i \tag{44}$$

or

$$\mathbf{M}\ddot{\mathbf{U}}^n + \mathbf{F}_T^n = \mathbf{F}_e^n, \tag{45}$$

where $\mathbf{M}$ is the lumped mass matrix, $\mathbf{F}_e^n$ is the external force vector, and $\mathbf{F}_T^n$ is the internal force vector. Each diagonal term of $\mathbf{M}$ is ρV_i and each component of $\mathbf{F}_e^n$ is $\mathbf{b}_i^n V_i$. Likewise, each component of $\mathbf{F}_T^n$ is $\sum_p \mathbf{f}(\mathbf{u}_p^n - \mathbf{u}_i^n, \mathbf{x}_p - \mathbf{x}_i) V_p V_i$, which is the sum of all the forces from the trusses connected to node i. Thus, the process of implementing peridynamics in an FEA code essentially boils down to a preprocessing task of generating a truss assembly (mesh) and stiffness properties for the trusses consistent with the peridynamic theory.

Although there are no technical issues with generating irregular peridynamic truss meshes, for simplicity only uniform rectangular meshes were used for the simulations presented in this paper. In this case a uniform rectangular array of nodes is first defined, and then trusses are generated by connecting any given node *i* to any other node *p* that lies within a sphere of radius δ centered at node *i*. Through the use of $\delta = 3\Delta x$, approximately 114 trusses are connected to each interior node of a three-dimensional body. Clearly, for even moderate-size problems, millions of trusses may be necessary if the entire region is modeled as peridynamic.

To alleviate some of the computational burden, it would be very desirable to couple a peridynamic truss mesh to a conventional FEA mesh. In this way, peridynamics could be used for the subregions where damage or fracture is expected, and the more efficient conventional FEA could be used for the remainder of the structure. Unfortunately, this coupling is not as simple as sharing nodes between meshes, as is commonly done in FEA. As previously mentioned, the boundaries in peridynamics are "fuzzy" (prescribed displacements or loads must be applied through a finite volume rather than on a surface). Thus, the coupling must be done over a region that spans some thickness, typically taken to be δ, from the exterior surface. This is most conveniently done by introducing a displacement constraint between the boundary of the peridynamic mesh and the FEA mesh boundary. If *p* denotes nodes within a distance δ of the peridynamic/conventional boundary, and *h* denotes the FEA nodes or elements to which they will be coupled, then the constraint is

$$\mathbf{u}_p = \mathbf{N}(a,b,c)\mathbf{u}_h, \tag{46}$$

where (a,b,c) are the parametric coordinates of the *p* nodes within or extrapolated from

the *h* elements, and **N** is the shape function matrix for the *h* elements. The constraint defined by Eq. (46) effectively enforces continuity of strain between the peridynamic mesh and the conventional FEA mesh. Since many general-purpose FEA codes permit constraint equations, Eq. (46) may be directly input, although the amount of data may be voluminous.

A more convenient way to couple the peridynamic and conventional parts of the FEA mesh is with embedded nodes and elements, which are available in the ABAQUS/Explicit computer code.[9] This capability makes the imposition of the constraint much easier. To use the embedded element feature, a band of thickness δ containing conventional continuum elements is defined to overlap the peridynamic trusses. The trusses are then specified to be embedded in the continuum elements. To keep the overlap region from being too stiff, the elastic modulus and density for the host continuum elements are set to very small values.

The definition of section and material properties for the peridynamic trusses is again a straightforward application of the theory. The mass of the nodes is defined via lumped masses as ρV_i, and the truss densities are set to zero. Because Eqs. (44) and (45) indicate that only the forces from the trusses connected to a given node are required, there is some nonuniqueness in the definition of the cross-sectional area A and elastic modulus E for the trusses. A convenient separation, which preserves the conventional units of these properties, is

$$A = \left(V_p V_i\right)^{1/3}, \quad E = c\left(V_p V_i\right)^{2/3}. \tag{47}$$

For a uniform rectangular mesh, then

$$A = \Delta x^2, \quad E = c\Delta x^4. \tag{48}$$

Also, as shown by Eq. (14), the bond stretch s is identical to the engineering strain in the trusses, thus the fracture strain of the trusses is

$$\boldsymbol{\varepsilon}_f = s_o \,. \tag{49}$$

For elastic-plastic materials, it can be shown that the strain s_y at which the bonds or trusses yield is related to Young's modulus E and the ultimate stress in tension σ_{ut} by

$$s_y \approx \frac{\sigma_{ut}}{2E} \,. \tag{50}$$

This implies that the macroscopic ultimate stress is about twice the yield stress for a pairwise force function in which the yielded part of the bond response is horizontal (Figure 2). This hardening phenomenon is a consequence of the fact that, in general, bonds in different orientations yield at different times during a process of macroscopic stretching of a body. For implementation in FEA, we set the truss element yield strain to $\varepsilon_y = s_y$ as determined by Eq. (50).

In contrast to EMU, in the current FEA implementation, the short-range forces are also restricted to the region within one horizon of each node. Thus, the contact interactions of Eqs. (32) through (34) are a simple modification of the compressive behavior of the trusses. For convenience this was implemented with a user-defined material in ABAQUS. More general application of the short-range forces consistent with EMU might be accomplished by a node-to-node contact algorithm. Unfortunately, this feature is not currently available in ABAQUS.

To complete the FEA model generation, the elastic modulus of the trusses that are within a distance δ of free surfaces needs to be modified by a normalization factor derived from Eq. (36). From Eqs. (36) and (47), the elastic modulus $E_b(\mathbf{X})$ of an element

near a boundary is

$$E_b(\mathbf{X}) = \frac{p_\infty^1}{p_\infty^1(\mathbf{X})} E . \tag{49}$$

For convenience of input into ABAQUS, we chose to capture this modulus variation near free surfaces with node-based, user-defined field variables.

Example Problems

Three example problems were chosen to demonstrate the accuracy and capability of peridynamics as well as the equivalency of the FEA implementation with the direct implementation contained in the EMU code. To effect meaningful comparisons, all problems were run in EMU and ABAQUS with the same uniform peridynamic grid and the same solution time step on a single processor of an SGI Prism 350 computer (eight 1.5 GHz Intel Itanium 2 processors with 20 GB RAM).

Brittle Center Cracked Plate

The first example, a classical fracture mechanics problem, is a brittle center cracked plate under a tensile load. The plate is 100 mm wide by 300 mm long by 10 mm thick, with a 50 mm through-thickness crack perpendicular to the long axis. The grid spacing is 2 mm, resulting in 37,500 nodes and approximately 1,700,000 trusses in ABAQUS. The material is aluminum with an elastic modulus of 68,900 MPa, a density of 2.7 g/cc, and a fracture toughness of 24 MPA-$m^{1/2}$. From Eq. (29), the fracture toughness was converted to the fracture strain for each truss. A prescribed displacement end load was ramped up over 5 msec to ensure quasi-static response before fracture. Figure 5 compares the center crack opening displacement and the far-field stress to the static handbook[10] solution and EMU. As is evident, both numerical implementations of peridynamics are within a few percent of the handbook solutions for the crack opening

displacement and the stress at fracture. It is interesting to note that there are some bond failures (as evidenced by the low-amplitude, high-frequency load oscillation) before fracture or unstable extension of the crack.

Plate Perforation

The second example is that of a rigid spherical ball impacting a ductile aluminum plate. The 5.11 kg ball is 50 mm in diameter, and the square plate is 250 mm on each side by 12.5 mm thick. The aluminum has a Young's modulus of 68,900 MPa, a density of 2.7 g/cc, and an ultimate strength of 310 MPa at 17% strain. The grid spacing is 2.5 mm, resulting in 50,000 nodes and approximately 2,400,000 trusses in ABAQUS. The sphere impacts normal to the plate at its center with a velocity of 500 m/sec.

In addition to a fully peridynamic FEA model of the plate, this example was also simulated using the coupled conventional/peridynamic FEA method described near Eq. (46). In the coupled model, the outer three-fourths of the plate consisted of 8-node reduced integration continuum elements. With this representation, there are 1200 conventional continuum elements, in addition to 12,500 peridynamic nodes and approximately 670,000 trusses. Thus, the coupled procedure greatly reduces the number of nodes and elements compared with the fully peridynamic FEA model.

Interaction between the spherical projectile and the plate is modeled using a kinematic contact algorithm. Figure 6 shows the acceleration history of the ball and the deformations shortly after the ball perforated the plate. Although there is no analytical solution to this problem, the plug formation and petaling are well-documented, experimentally observed features of this type of impact event.[11] The comparisons of FEA to EMU in both deformation and acceleration are within a few percent of each other, and

there is very little difference (except in run times) using the mesh coupling technique.

Projectile Penetration

The final example is that of a rigid projectile penetrating a cube of metal. From a model size and deformation viewpoint this was the most taxing of the three examples. Indeed, the ABAQUS preprocessor effectively limited the model to around 5 million trusses. The aluminum target was a 400 mm cube. The aluminum had the same properties as in the perforation example. The grid spacing of 10 mm resulted in 64,000 nodes and approximately 5,000,000 trusses in ABAQUS. Because large motion of the particles was anticipated, a limited number of additional compression-only trusses were added to the nodes in the path of the penetrator to permit short-force interaction outside of the horizon. The penetrator was 100 mm in diameter and 300 mm long, with a 3 CRH (caliber radius head) ogive nose. The penetrator mass was 15 kg, and it impacted the target at 700 m/sec. Again, interaction between the projectile and the target was captured with a kinematic contact algorithm. EMU accounts for the node radii in the contract algorithm for this type of projectile, so that for purposes of the contact algorithm for a rigid penetrator in EMU, each node acts like a hard sphere. Since the ABAQUS code does not account for a node radius, the dimensions of the projectile are increased by the diameter of the nodes (the grid spacing) in the FEA simulations to compensate for this. Figure 7 compares the resulting deformations and acceleration of the penetrator. Here, the peak penetrator accelerations predicted by EMU and FEA are again within a few percent, although there is a slight difference in the character of the penetrator acceleration history and the target deformation. These differences may be due to the limited span of the short-range forces in the FEA implementation or the lack of node radii in the FEA contact.

It is noted that in both this and the previous examples, the peridynamic FEA simulations never suffered from any of the numerical problems (mesh entanglement, advection anomalies, etc.) that one might expect with conventional (partial differential equation) continuum mechanics approaches. (Since EMU is meshless, the issue of mesh entanglement does not arise.) Freedom from these types of pathological behavior appears to be a key advantage of our approach.

As the examples demonstrate, there are no substantial differences in results between the direct and FEA implementations of peridynamics, although there appear to be some significant differences in computational efficiency. Table I compares computer wall-clock run times between the direct and FEA simulations. It is noted that these run times are measured with no competition with other jobs, i.e., no other jobs were running on the processor during the time that EMU or ABAQUS was executing. As is evident, the FEA (ABAQUS) implementation is dramatically faster than the direct meshless approach (EMU). On the other hand, even though the memory usage could not be precisely quantified it appears that EMU is almost an order of magnitude less demanding of physical memory than ABAQUS in most cases.

Conclusions

The theoretical basis for peridynamics together with the numerical implementation and examples presented in this paper clearly demonstrate**s** that this approach has very attractive and robust capabilities for problems involving damage and fracture. A key advantage of the peridynamic approach is its ability to model individual cracks that grow and interact with each other in arbitrarily complex patterns. The method is designed to reproduce a prescribed energy release rate that is characteristic of the

material in which a crack is growing. It is also applicable to interface fractures.

Numerical implementation of the peridynamic equations leads to the meshless method used in the EMU code. However, since we have shown that the technique can easily be adapted and coupled to conventional finite element analysis with no loss of computational efficiency (and perhaps with some significant speed gains), a much broader range of structural problems is now within the reach of the practicing engineering analyst. We have also demonstrated that the resulting FEA implementation of peridynamics in the ABAQUS code leads to essentially the same results as EMU in problems in which both methods are applicable. As demonstrated here, an FEA model can include both a peridynamic and conventional finite element subregions whose boundary is conveniently set up using embedded elements.

The FEA implementation of peridynamics is expected to be especially useful in penetration modeling because it avoids many of the well-known difficulties in describing the interface between a penetrator and a target when using conventional finite elements. In particular, the use of truss elements to describe the target is expected to reduce or eliminate problems with mesh tangling and distortion.

Acknowledgments

This work was supported by the United States Department of Energy and by the Joint US DOE/DoD Munitions Technology Program. Sandia is a multiprogram laboratory operated by Sandia Corporation for the United States Department of Energy under contract DE-AC04094AL85000.

References

1. S. A. Silling, "Reformulation of elasticity theory for discontinuities and long-range forces," *Journal of the Mechanics and Physics of Solids* **48**, 175–209 (2000).

2. S. A. Silling, M. Zimmermann, and R. Abeyaratne, "Deformation of a peridynamic bar," *Journal of Elasticity* **73**, 173–190 (2003).

3. S. A. Silling and E. Askari, "Peridynamic modeling of impact damage," in *Problems Involving Thermal-Hydraulics, Liquid Sloshing, and Extreme Loads on Structures,* F. J. Moody, Ed., New York: American Society of Mechanical Engineers, PVP-Vol. 489, pp. 197–205 (2004).

4. S. A. Silling and E. Askari, "A meshfree method based on the peridynamic model of solid mechanics," *Computers and Structures* **83**, 1526–1535 (2005).

5. S. A. Silling and F. Bobaru, "Peridynamic modeling of membranes and fibers," *International Journal of Non-Linear Mechanics* **40,** 395–409 (2005).

6. O. Weckner and R. Abeyaratne, "The effect of long-range forces on the dynamics of a bar," *Journal of the Mechanics and Physics of Solids* **53,** 705–728 (2005).

7. S. A. Silling, *EMU Theory Manual (*in preparation).

8. L. Lapidus and G. F. Pinder, *Numerical Solution of Partial Differential Equations in Science and Engineering*, New York: Wiley, p. 171 (1982).

9. *ABAQUS/Explicit Version 6.6 User's Manual*, Providence, Rhode Island: ABAQUS Inc. (2006).

10. H. Tada, *The Stress Analysis of Cracks Handbook*, St. Louis: Del Research Corporation, pp. 2.1–2.3 (1973).

11. W. Johnson, *Impact Strength of Materials*, London: Edward Arnold, pp. 138–146, 330–336 (1972).

Figures

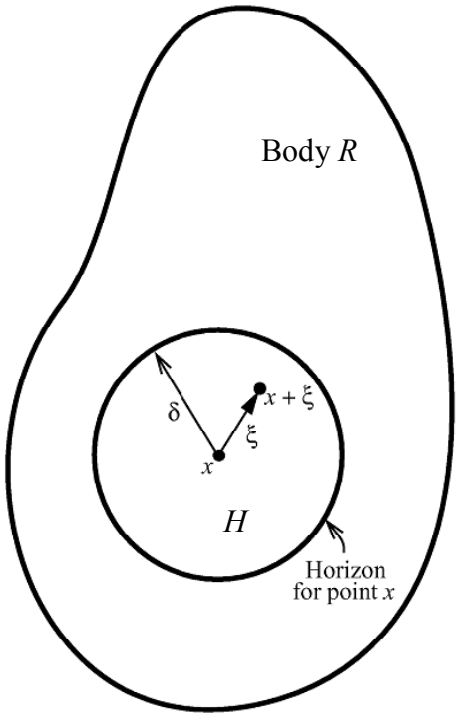

Figure 1. Each point **x** in the body interacts directly with points in the sphere $H_{\mathbf{x}}$ through bonds.

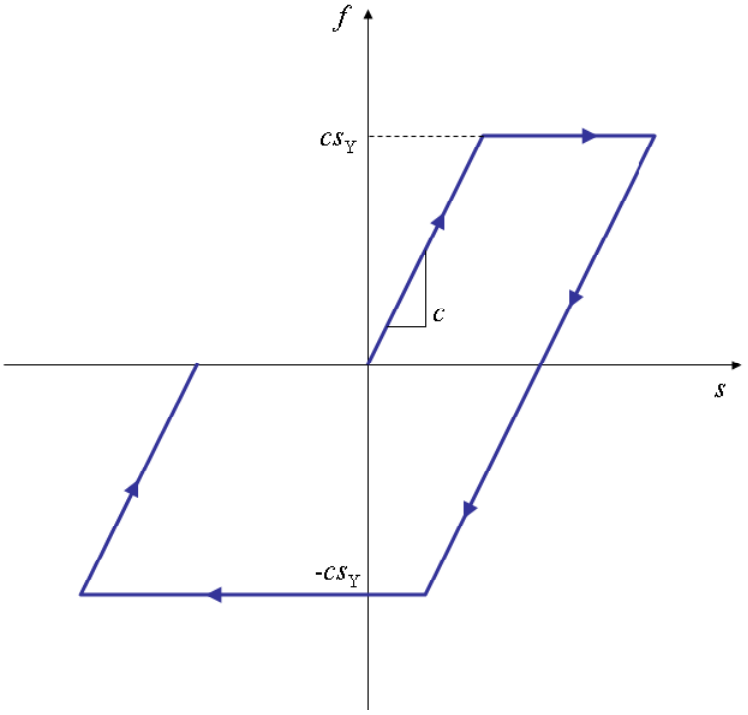

Figure 2. Bond force as a function of bond stretch in the proportional microplastic material for a possible loading path (tension followed by compression). This loading path results in a permanent compressive strain in the bond.

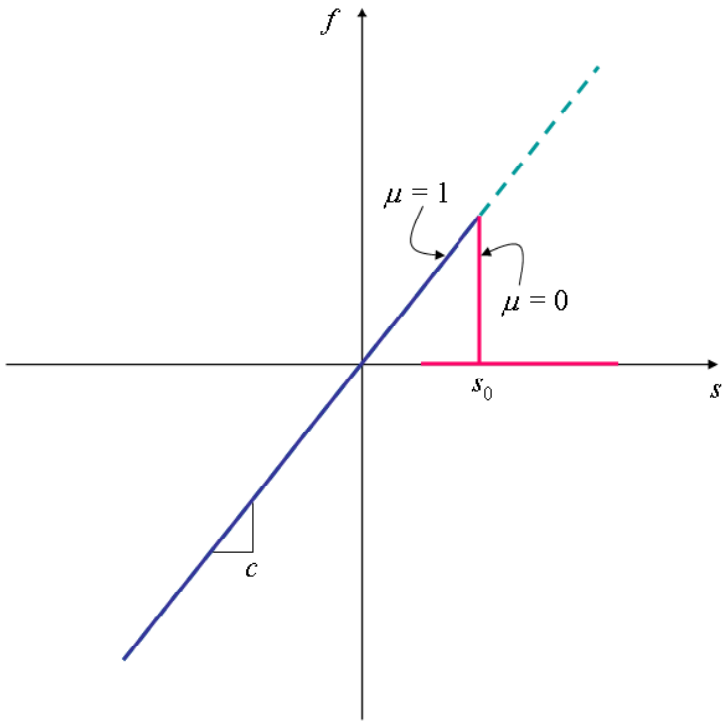

Figure 3. Bond force as a function of bond stretch in the PMB material, showing bond breakage at stretch s_0.

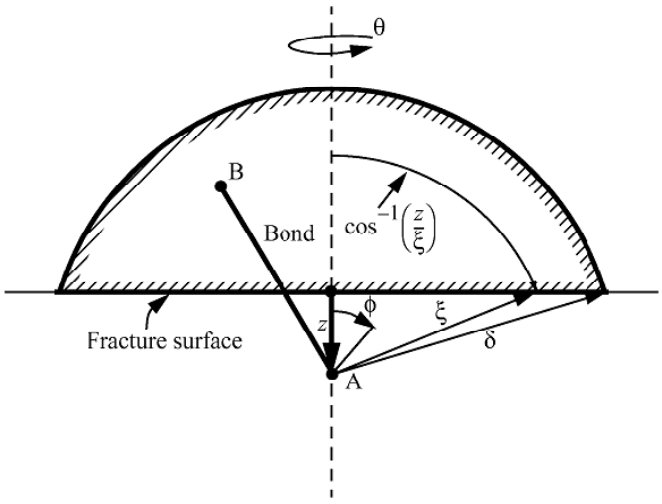

Figure 4. Integration over all bonds connecting two half-spaces determines the energy per unit area required to advance a crack.

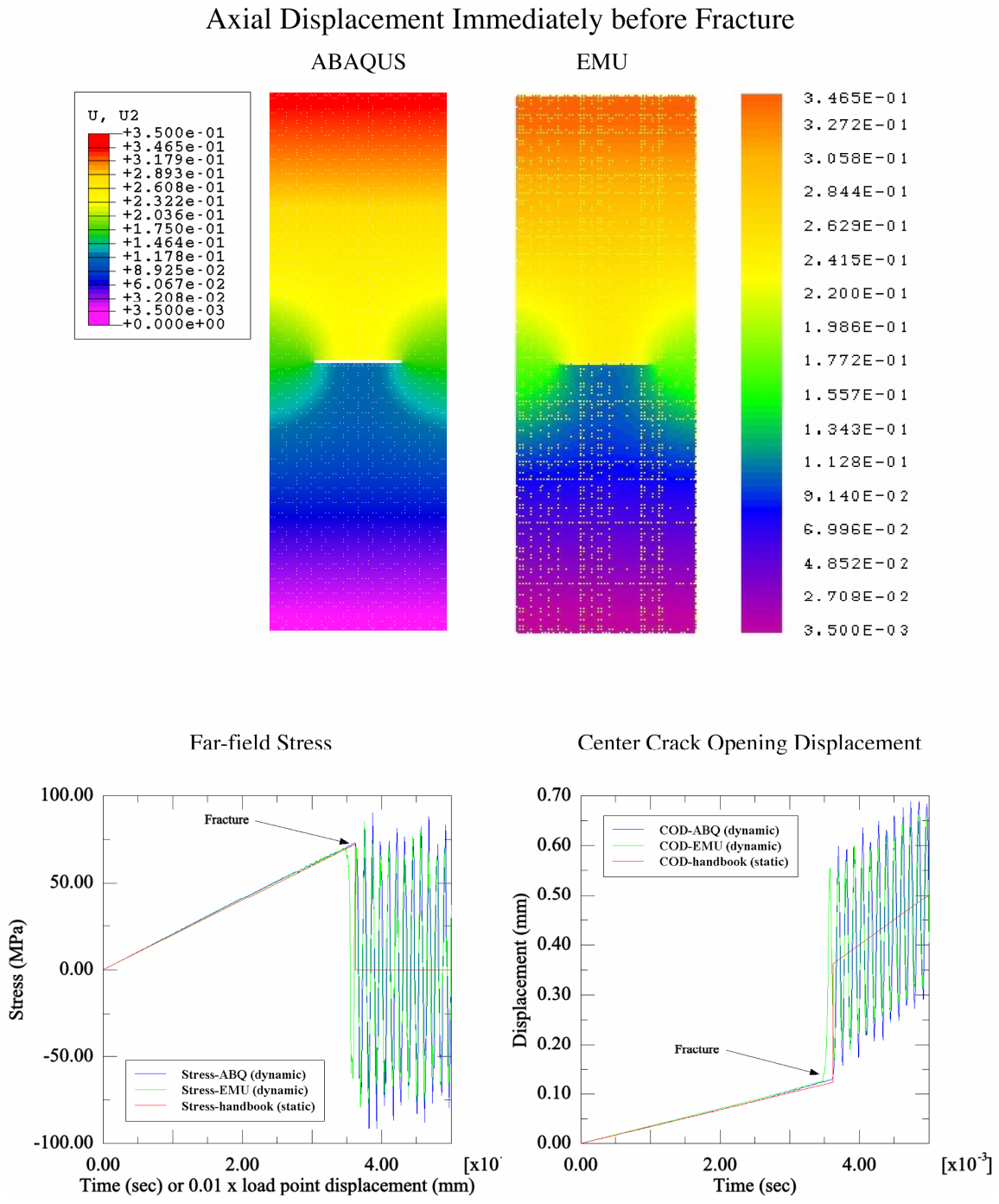

Figure 5. Deformation and response histories for the center-cracked plate example.

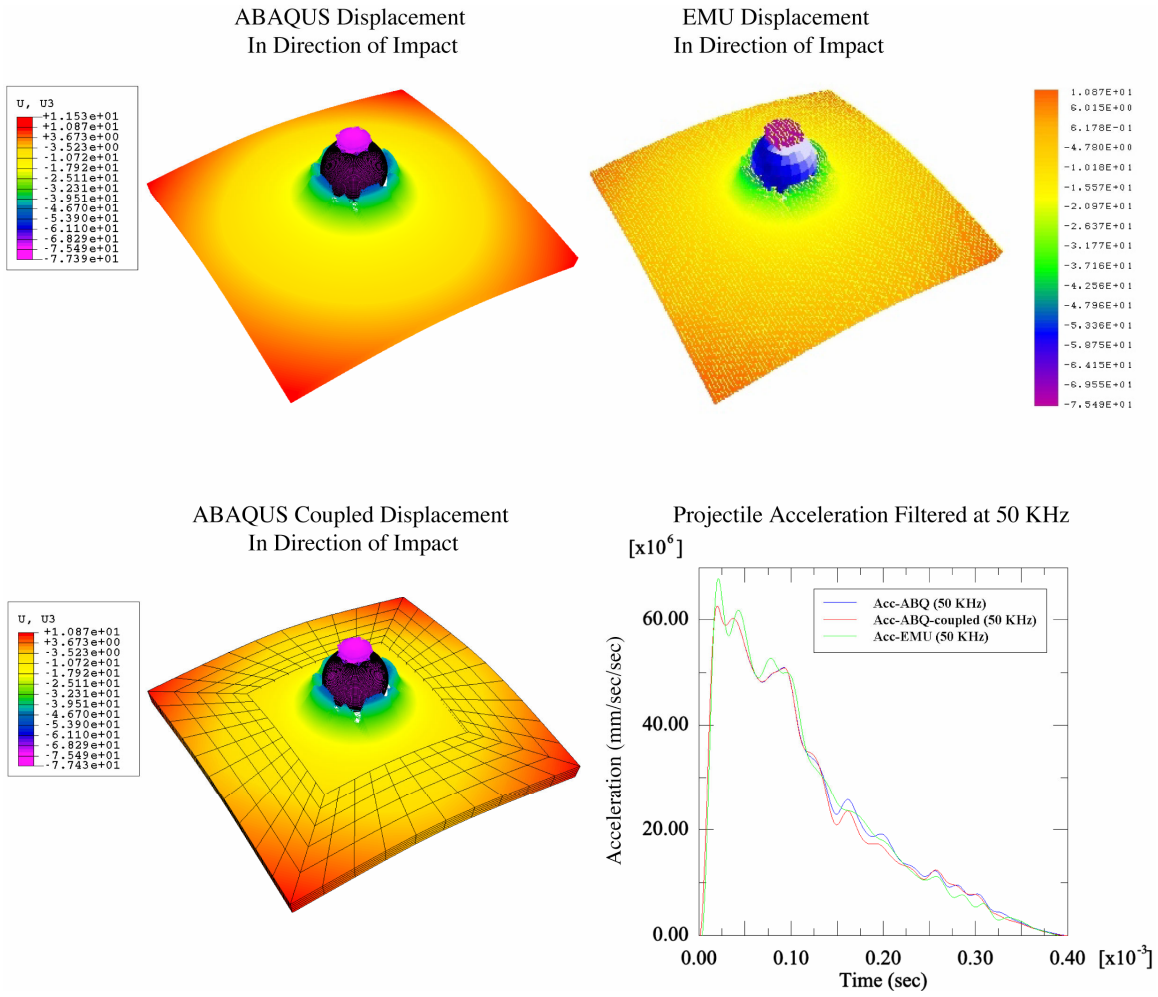

Figure 6. Deformations and projectile acceleration for the plate perforation example.

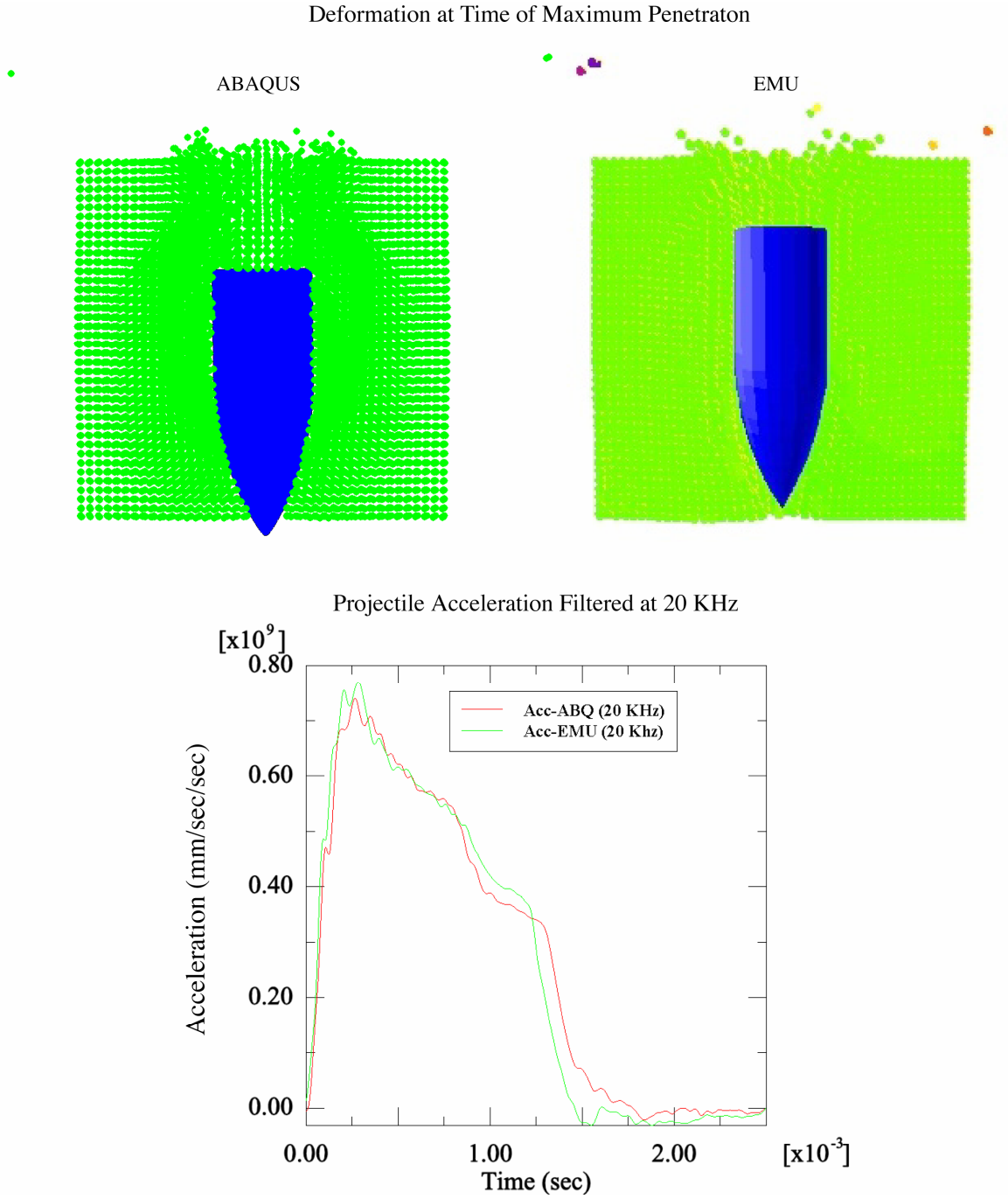

Figure 7. Deformations and projectile acceleration for the projectile penetration example.

Tables

Table I. Computer Run-Time Comparisons on a Single Processor of an SGI Prism 350 Computer.

Example problem	Approximate model size (nodes/elements)	Solution time step (μsec)	Wall-clock run times (minutes)	
			EMU	ABAQUS
Center cracked plate	37,500/1,700,000	0.25	2255	350
Plate perforation	50,000/2,400,000	0.20	283	73
Plate perforation (coupled)	12,500/670,000	0.20	-----	27
Cube penetration	64,000/5,000,000	0.50	1328	294